PHYSICAL REVIEW C VOLUME 45, NUMBER 6 JUNE 1992

Transition densities of collective excitations in ^{118}Sn

J. E. Wise
Nuclear Physics Laboratory, Department of Physics, University of Colorado, Boulder, Colorado 80309

J. P. Connelly,* F. W. Hersman, J. H. Heisenberg, W. Kim, and M. Leuschner
University of New Hampshire, Durham, New Hampshire 03824

S. A. Fayans, A. P. Platonov, and E. E. Saperstein
I. V. Kurchatov Institute of Atomic Energy, Moscow 123182, Russia

V. Yu. Ponomarev
Laboratory of Theoretical Physics, Joint Institute for Nuclear Research, Dubna, Head Post Office, P.O. Box 79, SU-101000 Moscow, Russia

(Received 13 January 1992)

Electron scattering cross sections have been measured for the elastic and the first 2^+,3^- and low-lying 4^+ excitations in ^{118}Sn. Forward angle data were taken for momentum transfers in the range $1.24 < q < 2.74$ fm^{-1} allowing the extraction of transition charge densities in a Fourier-Bessel analysis. Comparisons are made with microscopic calculations performed in the framework of the self-consistent finite Fermi system theory and quasiparticle phonon approach.

PACS number(s): 25.30.Dh, 27.60.+j, 21.10.Re, 21.60.Ev

I. INTRODUCTION

In the excitation spectra of most even-even spherical nuclei there are low-lying excitations that can be described in a collective model of the nucleus as a vibration of the nuclear surface. The longitudinal electromagnetic response of such transitions in this model will then be surface peaked. Experimentally extracted transition charge densities from inelastic electron scattering experiments, however, show that low-lying quadrupole excitations may have considerable interior structure. In some cases interior structure is an indication of a small number of particle-hole transitions participating in the excitation. Thus, phenomenologically, the shape of the experimental densities can be explained as an admixture of the single particle motion coupled to the collective surface vibrations. Within the framework of self-consistent approaches, both modes of excitation are jointly incorporated, the surface peak being a coherent sum of a large number of particle-hole excitations and the volume structure corresponding to a contribution of a few isolated low-energy transitions. In nonmagic nuclei, the two-particle (two-hole) channel is strongly mixed with the particle-hole one influencing mainly the volume response. The interplay between collective and single-particle modes exhibited by low-lying quadrupole excitations has been experimentally investigated in Ref. [1] (for ^{89}Y), Ref. [2] (^{88}Sr), and Ref. [3] (^{204,206}Pb). In these cases it was shown that the transition densities of collective excitations in neighboring nuclei possess a very similar surface behavior, while the volume structure changes considerably from one nucleus to another. It is thus apparent that a detailed study of the transition charge densities of low-lying excitations can give insight into their microscopic structure.

The present work on the low-lying, bound state structure of ^{118}Sn belongs to a series of works on the detailed study of the transition charge densities of low-lying collective states in spherical, superfluid nuclei using high-resolution inelastic electron scattering. In a preceding paper [4], a number of such densities in ^{142}Ce were extracted from the experimental data and compared with predictions of the quasiparticle-phonon approach (QPA) and the finite Fermi system (FFS) theory. The analysis revealed a rather complex structure for the majority of states due to strong anharmonicity effects. Such a situation is typical for the nonmagic spherical nuclei with a soft collective quadrupole mode when the 2_1^+ state has comparatively low energy (0.64 MeV in ^{142}Ce).

The situation with semimagic nuclei is simpler. In such nuclei the 2_1^+ state lies higher (typically greater than 1 MeV), its collectivity is lower and the anharmonicity effects are less pronounced than in nuclei with both shells open. For this reason, the chain of tin nuclei ($Z=50$) has often been chosen as a touchstone for checking methods for the description of the pairing effects on the ground state nuclear properties [5–7]. These isotopes are also of special interest in the study of one-phonon states in superfluid nuclei. An adequate description of such simple one-phonon states should serve as a good basis for the analysis of more complicated cases.

*Present address: Department of Physics, Catholic University of America, Washington, D.C. 20064.

In this work we present the first extraction of the transition charge density for the lowest-lying collective excitations in ^{118}Sn from electron scattering data. Form factors and transition charge densities have been extracted for the first quadrupole excitation at 1.230 MeV, the first octupole transition at 2.328 MeV, and the lowest-lying hexadecapole transitions at 2.280 and 2.489 MeV. In addition, we have extracted the ground state charge distribution from a combined analysis of all available electron scattering data and muonic x-ray transition data. Our experimentally extracted densities are compared with calculations in the framework of the QPA and FFS theory. QPA calculations [8–10], which have been successfully applied to the description of the contribution of one- and two-phonon configurations to the transition charge densities of low-lying states in the $N=82$ region [4,11], are carried out here using the "standard" QPA technique with a phenomenological Woods-Saxon potential and separable multipole-multipole forces, with strength constants fitted to the position of the first state for each multipolarity. Calculations in this work performed within the framework of the FFS theory use the mixed (r,λ) representation as described in Refs. [4] and [12], but have been extended in the present work by the completion of completely self-consistent FFS calculations with the use of the finite-range density-dependent forces of Refs. [7,13]. These calculations have had considerable previous success in predicting the ground state properties of both magic and nonmagic superfluid nuclei.

II. EXPERIMENT AND DATA ANALYSIS

Forward angle electron scattering data have been taken covering a momentum transfer region of $1.24 \leq q \leq 2.74$ fm^{-1} using incident electron beam energies of 252 and 376 MeV at the MIT–Bates Electron Linear Accelerator Center. Data were accumulated using the Energy Loss Spectrometer System (ELSSY) [14] obtaining resolutions of 16 keV for the 252 MeV data and 25–30 keV at the 376 MeV incident energy.

Position information in the bend plane of the spectrometer was obtained from a pair of vertical drift chambers (VDC's) [15], while signals from two multiwire proportional chambers provided a determination of the particle trajectory in the transverse plane. These detectors were located at the approximate position of the spectrometer focal plane. Fiducial signals were initiated by a coincidence between a plastic scintillator detector and a gas Cherenkov counter, which also provided particle identification for the relativistic electrons. Corrections for aberrations due to the curvature of the spectrometer focal plane, kinematic recoil, and instrumental deadtime were made in an off-line analysis. Final spectra had typical energy resolutions of $\delta E/E = 8\times10^{-5}$.

Cross sections were determined from electron energy loss histograms using the line-shape fitting program ALLFIT [16]; the line shape was taken as the convolution of a Gaussian and the theoretical line shape due to radiative processes [17]. Energy calibrations were determined using the differential recoil from known excitations in isotopes of varying mass. Using this method, the incident beam energies were determined to be 252.2±0.3 and 376.4±0.4 MeV. Data were taken over an angular range of 58°–78.6° at 252 MeV and 47°–80° at 376 MeV. Shown in Fig. 1 is a spectrum of inelastically scattered electrons from ^{118}Sn showing several of the low-lying excitations. The incident electron energy for these data is 252 MeV and the laboratory scattering angle is 68°. The data shown have been histogrammed into 5 keV bins and known excitations [18] have been line-shape fit to obtain the differential cross section for each level.

To aid in the extraction of the densities low momentum transfer data from Yale [19] and NIKHEF-K [20,21] were added to the analysis procedure.

Data were taken using target foils of 97.8% isotopically enriched ^{118}Sn. Targets of 10.48 and 19.86 mg/cm^2 thickness were used. As the melting point of tin is relatively low (231.9 °C), the target foils were rotated in the beam to spread the flux over a large enough area to prevent melting. This also had the advantage of averaging over target thickness irregularities.

Cross sections have been measured for levels up to 4.0 MeV. In this paper we present the experimentally extracted radial charge distribution for the ground state, as well as the transition charge densities for the first excited quadrupole, octupole, and hexadecapole levels in ^{118}Sn.

Elastic cross sections extracted from the present work, along with cross sections from previous (e,e') experiments [19–24] and Barrett moments obtained from muonic x-ray experiments [25], were fit in a Fourier-Bessel analysis of the nuclear ground state [26,27]. The reduced χ^2 for this fit to all data was 1.2 per degree of freedom. Shown in Fig. 2 is the extracted charge form factor, $|F^C|^2$, defined as the differential scattering cross section divided by the Mott cross section for unit charge and the recoil factor $\eta_{\rm rec}$, where

$$\eta_{\rm rec} = \left[1+\frac{2E_i\sin^2(\theta/2)}{M_t c^2}\right]^{-1} \tag{2.1}$$

and

$$\left[\frac{d\sigma}{d\Omega}\right]_{\rm Mott} = \frac{\alpha^2(\hbar c)^2\cos^2(\theta/2)}{4E_i^2\sin^4(\theta/2)}\ , \tag{2.2}$$

where M_t is the mass of the target nucleus.

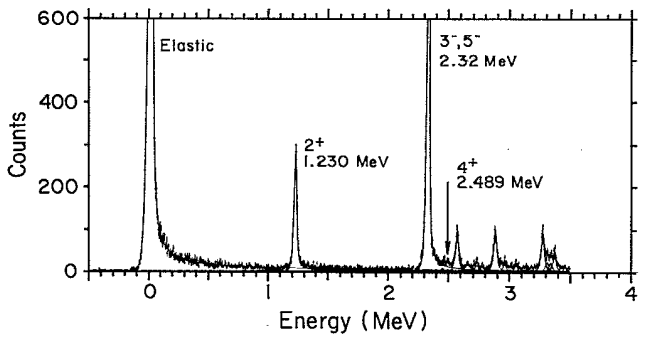

FIG. 1. Spectrum of inelastically scattered electrons from ^{118}Sn at 252 MeV, 68° ($q_{\rm eff}=1.48$ fm^{-1}) showing levels below 4.0 MeV excitation.

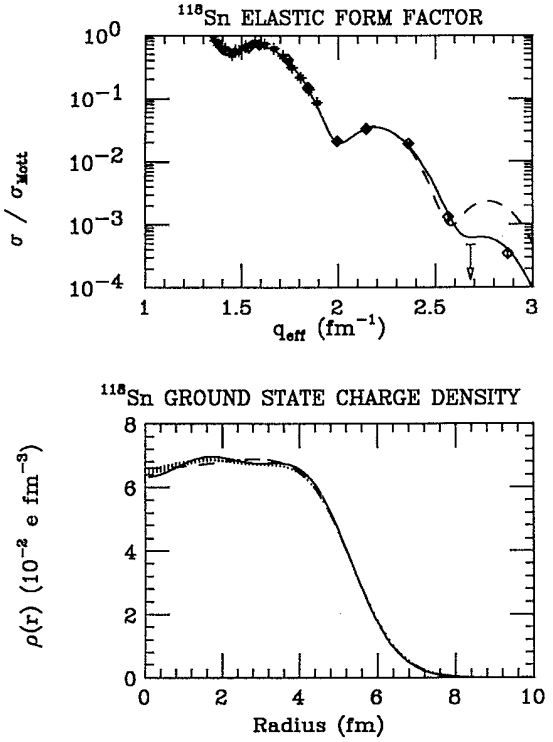

FIG. 2. Top: Elastic form factor (cross section divided by Mott cross section) for ^{118}Sn recalculated to 376.4 MeV with best fit from DWBA phase shift calculations (solid line). Dashed line is the prediction based on a three-parameter Gaussian model for the ground state density. Bottom: Ground state charge distribution as extracted in the Fourier-Bessel analysis. Dashed line is a best fit Gaussian parametrization while the solid line is the FFS calculation discussed in the text.

The solid line is the best fit distorted wave Born approximation (DWBA) form factor recalculated to an incident energy of 376.4 MeV, while the dotted line shows the form factor obtained from a DWBA calculation where the density has been parametrized as a three parameter Gaussian:

$$\rho_0(r)=\rho_0\frac{1+w(r/c)^2}{1+\exp[(r^2-c^2)/z^2]} . \tag{2.3}$$

Here the fitted parameters are $w=0.304\pm0.012$, $c=5.072\pm0.007$ fm, and $z=2.693\pm0.003$ fm as taken from Ref. [23]. Although the present analysis includes a total of 66 cross section measurements spanning a momentum transfer range of $0.49<q<2.74$ fm^{-1}, we have plotted only those data that cover the region of momentum transfer covered by the Bates measurements. Except for the region of high momentum transfer, $q>2.5$ fm^{-1}, this Gaussian parametrization describes the data rather well. The ground state charge density extracted in the Fourier-Bessel analysis is shown in the bottom of Fig. 2, along with this three parameter Gaussian fit (dashed line). The parametrization averages over the small interior oscillations, but is seen to give an overall good description of the size and shape of the experimental density. Calculations performed within the framework of the FFS theory are shown as the solid line in this figure. The interior structure, which was not reproduced by the Gaussian parametrization, is qualitatively produced by this calculation, though the surface is somewhat enhanced as compared to the experimentally extracted density.

The rms radius of the charge density as derived from the present analysis is found to be $\langle r_{ch}^2\rangle^{1/2}=4.6424\pm0.0007$ fm. This compares with the previous experimental extraction [28] for the rms radius of $\langle r_{ch}^2\rangle^{1/2}=4.648\pm0.007$ and a calculated value of 4.6104 fm in the FFS model.

Inelastic cross sections obtained in this work have been normalized to the elastic scattering cross sections of ^{118}Sn. Best fits in the Fourier-Bessel analysis to all scattering cross sections and muonic x-ray data provided separate normalization factors for each energy and angle. Typical normalizations were 6% for the Bates data. These normalizations have been applied to the fitted data to provide the final cross sections presented in this work.

III. INELASTIC EXCITATIONS

Laboratory cross sections obtained for the inelastic excitations in ^{118}Sn have been analyzed to extract the transition charge density in the Fourier-Bessel analysis [29]. In this method the transition charge density is expanded into a Fourier-Bessel series [29] given by

$$\rho_L(r)=\sum_{\mu=1}^{N} A_\mu q_\mu^{L-1} j_L(q_\mu^{L-1} r) \tag{3.1}$$

for $r<R_c$. Here the densities are zero for radii greater than the cutoff radius R_c, where $R_c q_\mu^L$ is the μth zero of the spherical Bessel function of order L.

The coefficients A_μ are determined in a least-squares fit to the calculated cross section in DWBA [30]. In the DWBA treatment, the distorted incoming and outgoing electron waves are given by a partial wave expansion, with the two component radial wave functions satisfying the Dirac equation for a spherically symmetric electric potential. Correct treatment of the Coulomb distortions is necessary for heavy nuclei such as ^{118}Sn and thus the simple relationship that exists between form factors and transition densities in the standard plane wave Born approximation (PWBA) does not exist in the present analysis. Matrix elements of the interaction Hamiltonian between initial and final nuclear states are calculated for the transition of multipolarity L with the nuclear currents related through the continuity equation:

$$\sqrt{2L+1}\left[\frac{\omega}{c}\right]\rho_L(r)=\sqrt{L}\left[\frac{d}{dr}-\frac{L-1}{r}\right]J_{L,L-1}(r) -\sqrt{L+1}\left[\frac{d}{dr}+\frac{L+2}{r}\right]J_{L,L+1}(r) . \tag{3.2}$$

Collective excitations in heavy nuclei, such as the 2^+ excitation in ^{208}Pb as discussed in Ref. [31], or the low-lying excitations in the rare-earth nuclei [4,11,32], are

seen to have little contribution from the transverse current $J_{L,L+1}(r)$. We anticipate this also to be true for the collective excitations in tin. To investigate the transverse contribution in ^{118}Sn, we have, in addition to the forward angle data, taken an inelastic spectrum at 155°, 252.4 MeV incident electron energy and compared the cross sections of several low-lying states to forward angle data taken at approximately the same value of momentum transfer. Rosenbluth separations give maximum transverse contributions of 2% for the first quadrupole transition at 1.230 MeV and 5% for the 4^+ excitation at 2.489 MeV. These percentages are consistent with the absence of a large transverse contribution. In the present work we have thus analyzed the cross sections assuming irrotational flow and thus requiring only those contributions from the current $J_{L,L-1}(r)$ as required by the continuity equation.

Shown in Fig. 3 are the scattering data for the 1.230 MeV 2^+ level recalculated [29] to an incident electron energy of 376.4 MeV, and plotted as a function of $q_{\rm eff}$, the effective momentum transfer. This is defined as

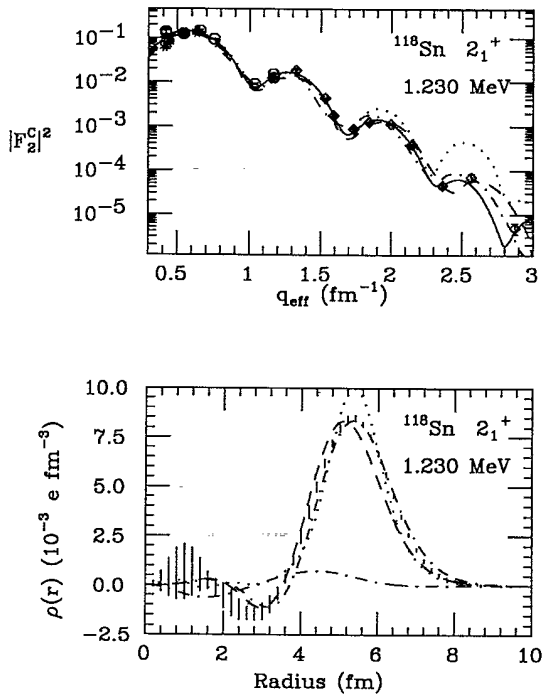

FIG. 3. Top: Charge form factor recalculated to 376.4 MeV with best fit (solid line) from DWBA phase shift calculation. Dotted line is the prediction of the Tassie model, dashed line FFS calculation, dot-dashed line QPA calculation. Data are from this work (diamonds), Ref. [19] (stars), and Ref. [20] (circles). Bottom: Transition charge density $\rho(r)$ for the first quadrupole transition at 1.230 MeV in ^{118}Sn. Error band is the best fit to the data in the Fourier-Bessel analysis; the dashed line is from a calculation using the self-consistent finite Fermi system theory; the dot-dashed line is the prediction of the quasiparticle phonon approach; dotted line is the Tassie model; small dot-dashed line at bottom of figure is the two-phonon component from the QPA model multiplied by a factor of 10.

$$q_{\rm eff}=q\left[1+\frac{4Z\alpha\hbar c}{3E_i r_0 A^{1/3}}\right], \tag{3.3}$$

where a radial parameter of $r_0=1.12$ fm has been used to define the nuclear size. The best fit to the scattering data in DWBA is shown as the solid line in the figure, where we have plotted the ratio of the measured cross section to the Mott cross section,

$$|F_L^C(q)|^2=\frac{d\sigma}{d\Omega}\Big/4\pi\eta_{\rm rec}\left[\frac{d\sigma}{d\Omega}\right]_{\rm Mott}.$$

Here $\eta_{\rm rec}$ and the Mott cross section are defined as in Eqs. (2.1) and (2.2). For longitudinal transitions in PWBA, this ratio is the square of the charge form factor for a transition of multipolarity L, and is thus the Fourier-Bessel transform of the transition charge density. Though this relationship is not correct in DWBA, if the transverse contributions are not great, all the data may be presented in a single figure by recalculating each cross section to the highest energy in DWBA and dividing by the elementary scattering cross section and kinematic factor.

The extracted transition charge density for these data is also shown in Fig. 3 along with three model calculations. Error bands include both statistical and incompleteness errors. From this density, the transition strength as given by the $B(E2)\uparrow$ value, defined for a transition of multipolarity L as

$$B(EL)\uparrow=\left|\frac{\sqrt{2J_f+1}}{\sqrt{2J_i+1}}\int_0^\infty\rho(r)r^{L+2}dr\right|^2, \tag{3.4}$$

is found to be $(1979\pm47)e^2$ fm^4. This is somewhat larger than obtained in previous low momentum transfer (e,e') data [19,20], where only the first maximum of the form factor was fit in a hydrodynamic model. These analyses obtained values of $(1722\pm50)e^2$ fm^4 and $(1560\pm60)e^2$ fm^4 (see Table I). Our analysis obtains a somewhat lower value, however, than the value of $(2160\pm50)e^2$ fm^4 obtained from Coulomb excitation experiments [33,34], or the pion scattering analysis of Ref. [35] which gives a value of $3350e^2$ fm^4 for the transition strength of the first 2^+ in ^{118}Sn.

Data have been analyzed to obtain the transition charge density for the first octupole level at 2.328 MeV. Analysis of these data was complicated by the presence of a weak, unresolved 5^- level which has been observed at 2.321 MeV in γ-decay experiments [18,36]. Our data were corrected for the additional $E5$ strength by using models of its contribution to the cross section from our calculations. Cross sections were calculated in both QPA and FFS for the first 3^- and 5^- levels and the corresponding form factors were scaled to give a best fit to the combined data at 2.32 MeV. The difference in the calculated cross section predicted in the two models was added to the final error as an estimate of the uncertainty in this procedure.

Previous results from (e,e') experiments [19,20] have been at low momentum transfers ($q_{\rm eff}\leq1.2$ fm^{-1}), and

TABLE I. Excitation energies and transition strengths of the low-lying collective excitations in ^{118}Sn obtained from experiment, along with corresponding QPA calculations and self-consistent FFS predictions.

	Experiment		FFS		QPA	
J^π	E_x (MEV)	$B(E\lambda)$ (e^2 fm$^{2\lambda}$)	E_x (MeV)	$B(E\lambda)$ (e^2 fm$^{2\lambda}$)	E_x (MeV)	$B(E\lambda)$ (e^2 fm$^{2\lambda}$)
2^+	1.230	$(1.979\pm0.047)\times10^3$	1.21	1.98×10^3	1.25	2.31×10^3
	1.23[a]	$(1.72\pm0.05)\times10^3$				
	1.23[b]	$(1.56\pm0.06)\times10^3$				
3^-	2.328	$(1.06\pm0.04)\times10^5$	2.61	1.01×10^5	2.98	1.25×10^5
	2.32[a]	$(1.12\pm0.03)\times10^5$				
	2.32[b]	$(1.7\pm0.3)\times10^5$				
4^+	2.280	$(3.2\pm0.3)\times10^5$	2.50	9.36×10^5	2.39	5.52×10^5
	2.489	$(2.80\pm0.33)\times10^5$	3.38	2.05×10^5	2.87	1.82×10^5
5^-	2.321[c]	$(6.7\pm5.5)\times10^7$	2.39	1.22×10^7	2.32	3.55×10^7

[a]Reference [20].
[b]Reference [21].
[c]Unresolved level.

did not resolve the two levels. Analysis of the 3^- in these two experiments assumed the combined cross section to have little contribution from the unresolved 5^- state at these values of the momentum transfer. This assumption is confirmed by our calculations.

As the contribution of the 5^- state to the total cross section is predicted to be less than 1% at the peak of the first maximum of the 3^- state, the error in predicting the strength of the 3^- state is small. The contribution of the 5^- contamination is, however, momentum transfer dependent. Although corrections to the data were less than a percent at the first maximum of the form factor, in the minima of the 3^- form factor the 5^- contribution is predicted to be virtually all of the observed cross section; only upper limits to the 3^- form factor can be obtained through this procedure at these values of the momentum transfer.

We present in Fig. 4 the corrected form factor obtained

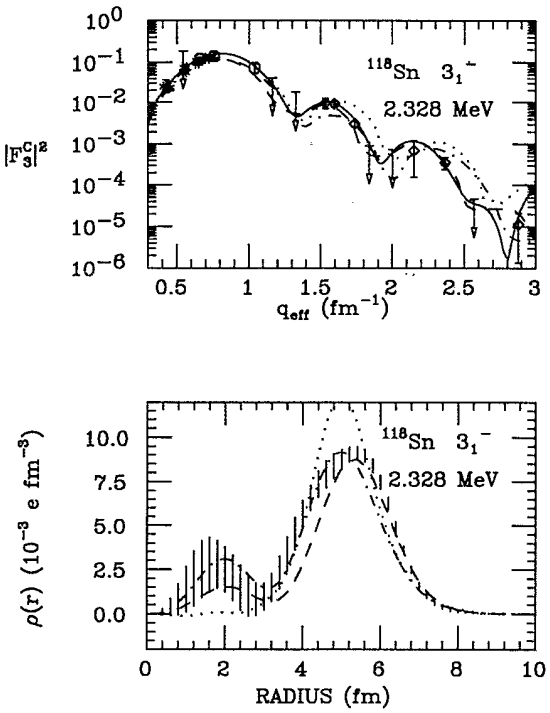

FIG. 4. Top: Charge form factor as defined in the text for the first 3^- excitation at 2.328 MeV. Best fit in DWBA is shown as solid line. Predictions of Tassie (dots), FFS (dashes), and QPA (dot-dashed) models are shown. Bottom: Transition charge density for first 3^- level. Curves are as listed in top figure.

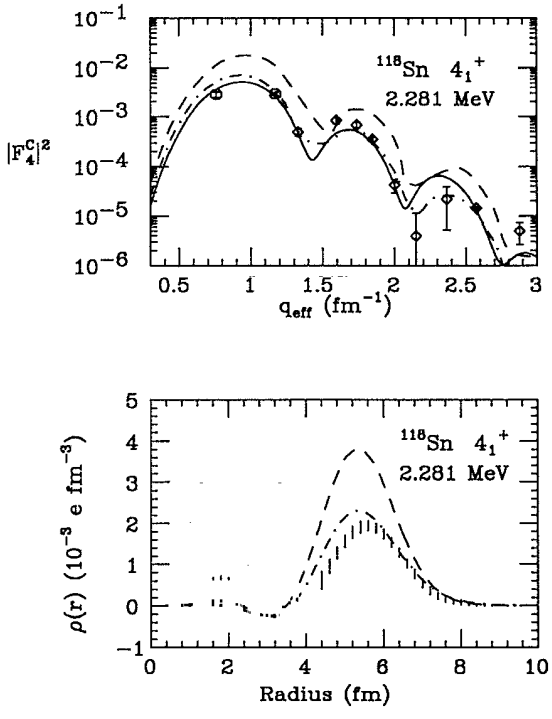

FIG. 5. Top: Charge form factor as defined in the text for the first 4^+ excitation at 2.280 MeV. Best fit in DWBA is given as solid line. FFS (dashed) and QPA (dot-dashed) calculations are also shown. Bottom: Transition charge density for first 4^+ level. Predictions of the one-phonon FFS (dashed) and QPA (dot-dashed) models are shown for the first 4^+.

with this procedure, and the model predictions. A Fourier-Bessel analysis of the corrected cross sections for the 2.328 MeV level, assuming $J^\pi=3^-$, gives the transition charge density displayed in the bottom half of Fig. 4. As can be seen in Table I, the experimental $B(E3)$ of $(1.06\pm0.04)\times10^5 e^2$ fm^6 is smaller than the previous values obtained from (e,e') data [19,20]. It is also found to be smaller than the value of 2.02×10^5 as extracted from the pion data [35], but is close to both the results predicted in the two theory calculations and to the value of $(9.7\pm1.4)\times10^4 e^2$ fm^6 obtained from Coulomb excitation [34]. By scaling the predicted form factors in QPA and FFS, we obtain an average for the transition strength of the unresolved 5^- level of $B(E5)=(6.7\pm5.5)\times10^7 e^2$ fm^{10}, where the large error is the result of the large difference between the predictions for the cross section in the two models. As the level is unresolved, this result should be treated as a highly model-dependent extraction of the transition strength. The transition strengths and excitation energies for these levels are listed in Table I.

The first and second excited 4^+ states lie at 2.280 and 2.489 MeV. Form factors and transition charge densities have been extracted for both of these excitations and are presented in Figs. 5 and 6. The relatively large errorbands on the two experimental densities reflect the limitations of the cross sections available for analysis, particularly at low momentum transfers. Both experimental densities show a large surface peak with a small interior lobe at about 2 fm, though the large experimental uncertainty in the interior precludes the positive identification of such an interior contribution. Experimental $B(E4)$ values and excitation energies are given in Table I.

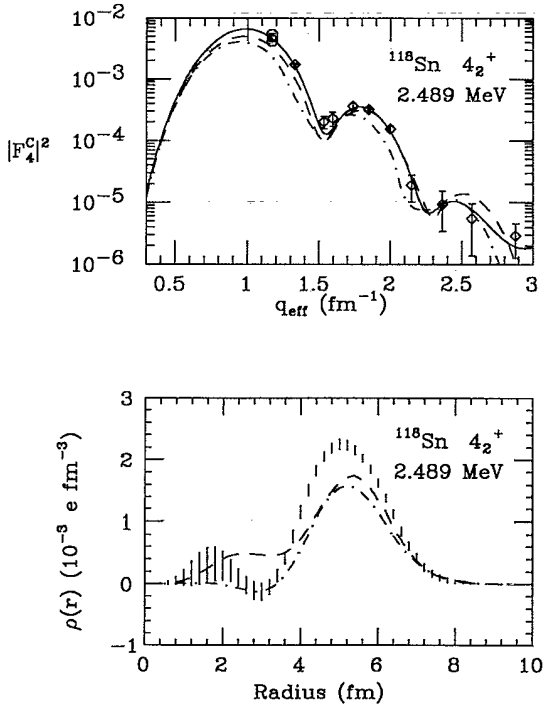

FIG. 6. Top: Charge form factor as defined in the text for the second 4^+ excitation at 2.489 MeV. Best fit in DWBA is given as solid line. FFS calculations (dashed), and QPA (dot-dashed) calculations are also shown. Bottom: Transition charge density for the second 4^+ level. Predictions of the one-phonon FFS model (dashed) and the QPA (dot-dashed) model are shown for the second 4^+.

IV. COMPARISON WITH MODEL CALCULATIONS

A. Tassie model

In the Tassie model [37] the excitations of the nucleus are described as small amplitude vibrations of an incompressible, irrotational fluid. To first order in the expansion amplitudes, the transition charge density for a transition of multipolarity L then has the form

$$\rho_L(r)\sim r^{L-1}\frac{d\rho_0(r)}{dr}\ , \tag{4.1}$$

where ρ_0 is the ground state charge density. Using the ground state charge density as extracted from the elastic scattering data, the transition density predicted in the modified Tassie model of Ref. [19] is given as the dotted line in the lower half of Fig. 3. The model density is surface peaked, with essentially no interior structure. The predicted shape is the result of the shape of the radial distribution of the ground state charge density, which is fairly uniform out to the nuclear surface at about 4 fm from the center, where it rapidly falls to zero.

The form factor calculated in DWBA using the density predicted in the Tassie model is shown as the dotted curve in the top half of Fig. 3. In this calculation, the strength of the transition has been adjusted to the best fit $B(E2)$ value of $1722e^2$ fm^4 found in Ref. [19]. The qualitative shape of the experimental form factor is reproduced by the model, but its size is overestimated by about an order of magnitude at high momentum transfer.

In Fig. 4 we present the form factor and transition charge density for the first 3^- level using the same modified Tassie model of Ref. [19], where the transition strength as given by the $B(E3)$ value is $1.12\times10^5 e^2$ fm^6. Although the form factor and surface peak of the transition charge density are again qualitatively reproduced by this phenomenological model, quantitative agreement with experiment in the nuclear interior is poor.

The Tassie model can be quantized and extended to higher orders in the expansion. In such vibrational models [29,38], the amplitudes become combinations of phonon annihilation and creation operators. Expanding the charge density in a Taylor series, it is found that the transition charge density for the n-phonon state is proportional to the nth derivative of the ground state charge density. Thus, interior structures not predicted in the Tassie model, such as are seen in the experimental densities of the 2_1^+ and 3_1^- levels, could be interpreted as admixtures of many-phonon contributions into the pure one-phonon state.

B. Quasiparticle-phonon approach

Microscopic calculations have been performed in the finite Fermi system (FFS) theory framework for collective

vibrations of superfluid nuclei and in the quasiparticle phonon approach (QPA) in order to determine the structure of low-lying states in ^{118}Sn. These models have had considerable success in predicting electron scattering transition charge densities for low-lying excitations in the $A=140$ region [4,11,32]. In the QPA, one-, two-, and three-phonon configurations are included in the wave functions of excited states and the interplay between these configurations is consistently taken into account. In this paper we include for each λ^π all one-phonon configurations up to an energy of 3 MeV, two-phonon configurations up to 7 MeV, and three-phonon configurations constructed of the first low-lying collective phonons. Since the model Hamiltonian is diagonalized in (λ) space, one may obtain information on the contribution of all these configurations to the structure of the excited states. The detailed description of this approach to the calculation of low-lying bound state transition charge densities can be found in Refs. [4,11]. The nucleus ^{118}Sn has a closed proton shell, and as our previous experience shows [11,32], the interaction between configurations of different complexity (i.e., between one- and two-phonon configurations, etc.) is not very strong for half-magic nuclei. This results in a more or less pure one-phonon structure for the lowest excitations and provides a justification for applying calculations within the one-phonon approximation.

In contrast to the $A=140$ region, in which we were dealing with open proton shell nuclei and the first one-phonon configurations had practically pure proton structure for half-magic isotopes [11,32] and proton-neutron structure for nonmagic isotopes [4,11], the tin isotopes with $Z=50$ have a closed proton shell. As a result the main two-quasiparticle configurations contributing to the structure of low-lying, one-phonon configurations are the neutron ones. For example, the main proton configuration for positive parity states is $\pi(1g_{9/2},2d_{5/2})$. This proton configuration gives a contribution of 8.2% to the structure of the first 2^+ one-phonon configuration but only 0.8% to the structure of the first 4^+ one-phonon configuration. Since electrons feel only the proton part of the phonon wave function, we obtain from the present experiment information only about the weak two-quasiparticle proton configurations in the structure of the low-lying phonons. However, as the surface behavior of the transition charge density of a collective excitation is largely determined by the coherent interference of many weak two-quasiparticle configurations, we obtain information about the collective aspects of an excitation from a study of the surface. It is found, for example, that the amplitude of the surface peak of the transition charge density of the first 2^+ state in closed proton shell nuclei has approximately the same value as in open proton shell nuclei [3]. On the other hand, the interior behavior of the transition density is often determined by the one or two strongest two-quasiparticle configurations and since such strong configurations do not exist in the low-lying phonons in ^{118}Sn, no pronounced peaks in the interior region appear in the present microscopic calculations. It is also not too surprising that no noncollective low-lying levels which are of neutron nature have been observed in the present experiment, contrary to the experiments in the $A=140$ region where several of them have been separated.

In the QPA calculation the first 2^+ state in ^{118}Sn has an excitation energy equal to 1.25 MeV and a $B(E2)\uparrow$ value of $2310e^2$ fm^4. The transition charge density of this state is shown by dot-dashed curves in Fig. 3. Though this state is a practically pure one-phonon state with 91% coming from the first one-phonon 2^+ configuration, some small admixture of two phonon configurations takes place. The main two-phonon configurations in this state are $[2_1^+\otimes 4_1^+]_{2^+}$ at 3.6% and $[2_1^+\otimes 2_1^+]_{2^+}$ at 2.1%. The influence of all two-phonon configurations on the shape of transition charge density is, however, very small and to present their contribution, shown by the small dot-dashed curve in the bottom of Fig. 3, we have had to multiply the curve by a factor of 10. The shape of the experimental density is well reproduced, though we have had to increase the value of the parameter r_0 of the Woods-Saxon potential from the value of 1.24 fm [39] to the value of 1.31 fm used in calculations for the $A=140$ region. The large $B(E2)$ in this calculation is a result of the shape of the Woods-Saxon well; the well produces a density that decreases more slowly than is experimentally observed in the exterior region of the nucleus. The same situation occurs in calculations with Woods-Saxon potentials for other half-magic nuclei [11].

The first 3^- state at 2.39 MeV in this calculation is again almost entirely due to the first one-phonon 3^- configuration (94% of the contribution). The shape of the predicted transition density, shown as the dot-dashed line in Fig. 4, is largely the result of this configuration. The second largest contribution to this state is from the $[2_1^+\otimes 3_1^-]_{3^-}$ two-phonon configuration (4.5%), and it contributes very little to the shape of the density. The $B(E3)\uparrow$ value of $1.25\times 10^5 e^2$ fm^6 is larger in this calculation than the experimental value. In this case it is not only that the shape of the Woods-Saxon well produces a density that is more slowly decreasing than the experimental density in the exterior region, as was the case for the 2_1^+ state, but the interior structure is also enhanced in the calculation, producing a transition strength slightly greater than is actually observed.

The situation with the 4^+ states is more complicated. The first one-phonon 4^+ configuration is less collective compared to the ones with $\lambda^\pi=2^+$ and 3^-. The second one-phonon 4^+ configuration is about 0.4 MeV higher and the shape of its transition charge density is very similar to the shape of the density for the first one-phonon 4^+ configuration. Both of these densities peak at approximately 5.3 fm, though the surface peak of the 4_2^+ is somewhat wider and has an amplitude about three times smaller than the 4_1^+.

The first two 4^+ levels are then the result of combinations of these configurations with closely lying two-phonon ones, producing states with excitation energies of 2.39 and 2.87 MeV and $B(E4)\uparrow$ values of $5.52\times 10^5 e^2$ fm^8 and $1.82\times 10^5 e^2$ fm^8, respectively. The first 4^+ state appears as a result of the coherent interference from the 77% contribution of the first one-phonon

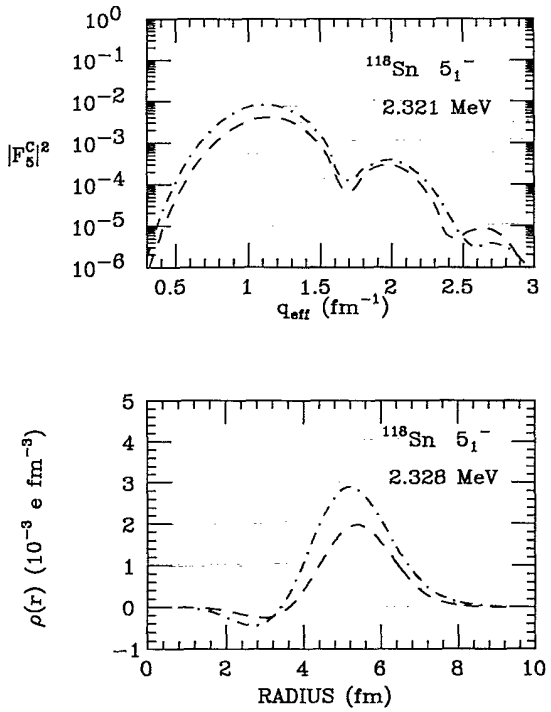

FIG. 7. Top: QPA (dot-dashed) and FFS (dashed) prediction for the form factor for the first 5^- excitation in ^{118}Sn. Bottom: Transition charge density for first 5^- level in ^{118}Sn as predicted in QPA (dot-dashed) and FFS (dashed).

4^+ configuration with the 16% contribution from the two-phonon configuration $[2_1^+ \otimes 2_1^+]_{4^+}$. In the structure of the second 4^+, the 83% contribution from the second one-phonon 4^+ configuration interferes destructively with the contributions of the two-phonon configurations (5% from $[2_1^+ \otimes 2_1^+]_{4^+}$ and 4% from $[2_1^+ \otimes 4_1^+]_{4^+}$). This interference results in the shift of the transition density maximum to 5.4 fm for the first 4^+ state and to 5.2 fm for the second. Such shifts are observed in the experimentally extracted densities. As can be seen from Figs. 5 and 6, the maximum of the peak of the first 4^+ is located at about 5.5 fm experimentally, while the maximum of the second 4^+ is found at approximately 5.0 fm.

In Fig. 7 we present the transition charge density and form factor predicted in the QPA for the unresolved 5^-. In this calculation the structure of the excitation is predicted to be largely one phonon, with a $B(E5)$ of $3.55 \times 10^7 e^2$ fm^{10}—consistent with the model-dependent extraction from the experimental data. In addition, we note the predicted excitation energy of 2.32 MeV is very close to the experimental value of 2.321 MeV.

C. Finite Fermi system calculations

Calculations of the bound state structure of ^{118}Sn presented in this work within the FFS framework use the mixed (r,λ) representation as described in Ref. [4] and Ref. [12] to solve the FFS theory equations for one-phonon states in superfluid nuclei. One essentially new ingredient is added in the present treatment: the nuclear mean field is generated self-consistently by the same effective forces which enter these equations. The effective finite-range forces are similar to those suggested in Ref. [7]. The only difference between the two forces is that those used in the present analysis contain a density-dependent surface term [13]. The ground state charge density ρ_0 obtained within this self-consistent approach is shown in Fig. 2.

It can be seen from Fig. 2 that the self-consistent FFS theory describes the ground state charge density quite well. The transition charge density for the first 2^+ state predicted in this approach is shown as the dashed curve in Fig. 3. Agreement with the experiment is also quite good. Both the calculated value of $E_x = 1.211$ MeV for the excitation energy and the predicted reduced transition probability of $B(E2)\uparrow = 1980 e^2$ fm^4 are in close agreement with the experimental values obtained for this state. It should be stressed that these calculations contain no adjustable parameters.

FFS calculations for the transition charge densities for the first 3^- and 4^+ levels are shown as dashed lines in Figs. 4–6. For the 3^- state agreement with experiment is again quite good; both the shape and strength as given by the $B(E3)$ value are within the errors of the experiment. $B(E3)$ values for the experiment and FFS calculations are given in Table I.

The interpretation of experimental data with the results of the FFS is complicated for the $L=4$ transitions observed in this experiment. In the FFS calculations at the one-phonon approximation level, we have found the two lowest 4^+ states to have excitation energies of 2.50 and 3.38 MeV with $B(E4)$ values of $9.26 \times 10^5 e^2$ fm^8 and $2.05 \times 10^5 e^2$ fm^8, respectively. Transition densities for the first two 4^+ levels in FFS are given as the dashed lines in Figs. 5 and 6. The shape of the calculated density for the first 4^+ agrees with experiment, but the model predicts enhanced interior structure for the 4_2^+ that is not seen in the experimental density. In addition, the FFS calculation predicts an energy separation of about 0.9 MeV between the two 4^+ excitations, but it is found experimentally that the first and second 4^+ states are separated by a small energy gap of only 208 keV. These results indicate that the density plotted for the FFS prediction for the second 4^+ in Fig. 6 may not correspond to the experimentally observed level at 2.489 MeV.

As the second experimentally observed 4^+ lies at almost exactly twice the energy of the first 2^+, one should expect that the mixing of one- and two-phonon components plays a more important role than predicted by the QPA calculations discussed above. One should then expect that both observed 4_1^+ and 4_2^+ states are superpositions of one-phonon 4_1^+ and two-phonon $[2_1^+ \otimes 2_1^+]$ configurations with approximately equal weights. The main strength would then come from the former, and this should result in two states with more or less similar transition densities and close $B(E4)$ values. A semiclassical estimate of the two-phonon $[2_1^+ \otimes 2_1^+]$ admixture shows that the $B(E4;0^+ \rightarrow 4_1^+)$ value is reduced to $4.05 \times 10^5 e^2$ fm^8 due to a destructive interference on the surface between the one- and two-phonon configurations,

with the surface peak being slightly shifted inward. Such a reduction in strength and inward shift of the maximum of the surface peak has been observed in the experimentally extracted densities. As for the second 4^+ state predicted in the FFS, it may correspond to one of the higher-lying levels reported to have $J^\pi=4^+$, such as the levels at 3.25 and 3.43 MeV [18], and this should be taken into account when looking at Fig. 6. To adequately describe the effects of mixing between one- and two-phonon configurations, microscopic self-consistent calculations within the FFS framework may be necessary. This will be the subject of a separate paper.

In Fig. 7 the FFS calculation for the form factor and transition charge density for the first 5^- state is shown as the dashed line. The shape predicted in the FFS theory for the density and form factor is very similar to that predicted by the QPA calculations; the predicted strengths, however, as measured by the $B(E5)$ values, differ from each other by approximately a factor of three (see Table I).

V. CONCLUSIONS

Data have been acquired and charge densities extracted for the ground state and first low-lying collective excitations in ^{118}Sn. This is a proton closed shell nucleus and transition charge densities of the low-lying states observed in this experiment are determined largely by collective phenomena. No noncollective, lowlying levels composed of practically pure neutron, two-quasiparticle configurations have been observed in this experiment. This is in contrast to what was found for the $A=140$ region, where several low-lying states determined to have a large two-quasiparticle component. The first quadrupole excitation of ^{118}Sn has little interior structure, while the higher multipolarities show interior structure consistent with the presence of more complex configurations. Microscopic calculations within the framework of the self-consistent finite Fermi system theory are able to reproduce the strength and shape of the ground state, 2^+ and 3^- excitations quite well. The quasiparticle phonon approach predicts these excitations to be largely one phonon in structure; the size and shape of the densities for these levels is well described in this model. On the other hand, the 4^+ states have a much more complicated structure. QPA calculations show these states to be combinations of one- and two-phonon configurations; calculations within this framework describe the experimental densities rather well. Calculations within the FFS framework at the one-phonon approximation level are not expected to describe the 4^+ states as well as the 2^+ and 3^- levels. Within this theoretical framework, a fully self-consistent treatment of the mixing with the two-phonon configurations may be necessary to adequately describe the extracted transition charge densities of the experimentally observed 4^+ excitations.

ACKNOWLEDGMENTS

The authors would like to thank the staff of the MIT–Bates Linear Accelerator for their help and support as well as R. J. Peterson, A. J. C. Burghardt, and J. H. Mitchell for release of data prior to publication. One of us (W.K.) would like to thank the Joint Institute for Nuclear Research and the Karchatov Institute of Atomic Energy for their support and hospitality during the visit. This work was supported in part by the U.S. Department of Energy under Contract No. DE-FG0-88ER40410.

[1] J. E. Wise, J. H. Heisenberg, F. W. Hersman, J. R. Calarco, J. Connelly, and C. Papanicolas, Phys. Rev. C **42**, 1072 (1990).
[2] J. Heisenberg, Comments Nucl. Part. Phys. **13**, 267 (1984).
[3] C. N. Papanicolas, J. Heisenberg, J. Lichtenstadt, J. S. McCarthy, D. Goutte, J. M. Cavedon, B. Frois, M. Huet, P. Leconte, Phan Xuan Ho, S. Platchkov, and I. Sick, Phys. Rev. Lett. **52**, 247 (1984).
[4] W. Kim, J. R. Calarco, J. P. Connelly, J. H. Heisenberg, F. W. Hersman, T. E. Milliman, J. E. Wise, B. L. Miller, C. N. Papanicolas, V. Yu. Ponomarev, E. E. Saperstein, and A. P. Platonov, Phys. Rev. C **44**, 2400 (1991).
[5] J. Decharge and D. Gogny, Phys. Rev. C **21**, 1568 (1980).
[6] M. V. Zverev and E. E. Saperstein, Yad. Fiz. **39**, 214 (1984) [Sov. J. Nucl. Phys. **39**, 878 (1984)].
[7] A. V. Smirnov, S. V. Tolokonnikov, and S. A. Fayans, Yad. Fiz. **48**, 1661 (1988) [Sov. J. Nucl. Phys. **48**, 995 (1988)].
[8] V. G. Soloviev, *Theory of Complex Nuclei* (Pergamon, Oxford, 1976).
[9] A. I. Vdovin and V. G. Soloviev, Fiz. Elem. Chastits At. Yadra **14**, 237 (1983) [Sov. J. Part. Nucl. **14**, 99 (1983)].
[10] V. V. Voronov and V. G. Soloviev, Fiz. Elem. Chastits At. Yadra **14**, 1380 (1983) [Sov. J. Part. Nucl. **14**, 583 (1983)].
[11] R. K. J. Sandor, H. P. Blok, U. Garg, M. N. Harakeh, C. W. de Jager, V. Yu. Ponomarev, A. I. Vdovin, and H. de Vries, Phys. Lett. B **233**, 54 (1989); Nucl. Phys. **A535**, 669 (1991); R. K. J. Sandor, Ph.D. thesis, University of Amsterdam, 1991.
[12] A. P. Platonov and E. E. Saperstein, Nucl. Phys. **A486**, 63 (1988).
[13] S. A. Fayans (unpublished).
[14] W. Bertozzi, M. V. Hynes, C. P. Sargent, W. Turchinetz, and C. Williamson, Nucl. Instrum. Methods **162**, 211 (1979).
[15] W. Bertozzi, M. V. Hynes, C. P. Sargent, C. Creswell, P. C. Dunn, A. Hirsch, M. Leitch, B. Norum, F. N. Rad, and T. Sasanuma, Nucl. Instrum. Methods **141**, 457 (1977).
[16] J. J. Kelly, C. E. Hyde-Wright, and F. W. Hersman, ALLFIT computer code (unpublished).
[17] J. Bergstrom, in *MIT 1967 Summer Study, Medium Energy Nuclear Physics with Electron Accelerators,* edited by W. Bertozzi and S. Kowalski (MIT, Cambridge, Massachusetts, 1967), p. 251.
[18] T. Tamura, K. Miyano, and S. Ohya, Nucl. Data Sheets **51**, 356 (1987).
[19] T. H. Curtis, R. A. Eisenstein, D. W. Madsen, and C. K. Bockelman, Phys. Rev. **184**, 1162 (1969).
[20] R. J. Peterson, J. J. Kraushaar, M. R. Braunstein, and J. H. Mitchell, Phys. Rev. C **44**, 136 (1991).

[21] A. J. C. Burghardt (private communication).
[22] V. M. Khvastunov, N. G. Afayasyev, V. D. Afanasyev, I. S. Gulkarov, A. S. Omelaenko, G. A. Savitsky, A. A. Khomich, N. G. Shevchenko, V. S. Romanov, and N. V. Rusanova, Nucl. Phys. **A146**, 15 (1970).
[23] J. R. Ficenec, L. A. Fajardo, W. P. Trower, and I. Sick, Phys. Lett. **42B**, 213 (1972).
[24] A. S. Litvinenko, N. G. Shevchenko, A. Yu. Buki, G. A. Savitsky, V. M. Khvastunov, A. A. Khomich, V. N. Polishchuk, and I. I. Chkalov, Nucl. Phys. **A182**, 265 (1972).
[25] R. Engfer, H. Schneuwly, J. L. Vuilleumier, H. K. Walter, and A. Zehnder, At. Nucl. Data Tables **14**, 509 (1974).
[26] B. Dreher, J. Freidrich, K. Merle, H. Rothhaas, and G. Luhrs, Nucl. Phys. **A235**, 219 (1974).
[27] Code MEFIT, B. Dreher and K. Merle, University Of Mainz (unpublished).
[28] E. Wesolowski, J. Phys. G **10**, 321 (1984).
[29] J. Heisenberg, in *Advances in Nuclear Physics,* edited by J. Negele and E. Vogt (Plenum, New York, 1981), p. 12; J. Heisenberg and H. P. Blok, in *Annual Review of Nuclear and Particle Science,* edited by J. D. Jackson, H. E. Gove, and R. F. Schwitters (Annual Reviews Inc., Palo Alto, CA, 1983), p. 569.
[30] H. C. Lee, Atomic Energy of Canada Limited Report AECL-4839, 1975, p. 2075.
[31] J. Heisenberg, J. Lichtenstadt, C. N. Papanicolas, and J. S. McCarthy, Phys. Rev. C **25**, 2292 (1982).
[32] W. Kim, B. L. Miller, J. R. Calarco, L. S. Cardman, J. P. Connelly, S. A. Fayans, B. Frois, D. Goutte, J. H. Heisenberg, F. W. Hersman, V. Meot, T. E. Milliman, P. Mueller, C. N. Papanicolas, A. P. Platonov, V. Yu. Ponomarev, and J. E. Wise, Phys. Rev. C **45**, 2290 (1992).
[33] P. H. Stelson, F. K. McGowan, R. L. Robinson, and W. T. Milner, Phys. Rev. C **2**, 2015 (1970).
[34] N. G. Jonsson, A. Backlin, J. Kantele, R. Julin, M. Luontama, and A. Passoja, Nucl. Phys. **A371**, 333 (1981).
[35] J. L. Ullman, P. W. F. Alons, B. L. Clausen, J. J. Kraushaar, J. H. Mitchell, R. J. Peterson, R. A. Ristenen, R. L. Boudrie, N. S. P. King, C. L. Morris, J. N. Knudson, and E. F. Gibson, Phys. Rev. C **35**, 1099 (1987).
[36] J. Hattula, E. Luikkonen, and J. Kantele, Z. Phys. **231**, 203 (1970); R. J. Gehrke and L. D. McIssac, United States Atomic Energy Commission Report ANCR **1088**, 379 (1972); A. Van Poelgeest, J. Bron, W. H. A. Hesselink, K. Allaart, J. J. A. Zalmstra, M. J. Uitzinger, and H. Verheul, Nucl. Phys. **A346**, 70 (1980).
[37] L. J. Tassie, Aust. J. Phys. **9**, 407 (1956).
[38] J. W. Lightbody, Jr., S. Penner, S. P. Fivozinsky, P. L. Hallowell, and Hall Crannell, Phys. Rev. C **14**, 952 (1976).
[39] V. Yu. Ponomarev, V. G. Soloviev, Ch. Stoyanov, and A. I. Vdovin, Nucl. Phys. **A323**, 446 (1979).